Attitude Stabilization of Flexible Spacecraft Using a Composite PD Approach

4.Attitude Stabilization of Flexible Spacecraft Using a Composite PD Approach

4.1. Introduction

As discussed in the previous chapter, high-precision attitude control of flexible spacecraft has been a complex problem, especially in communication, navigation, remote sensing, and other space-related missions. Modern Spacecraft often employ large, deployed, and lightly damped structures (such as solar paddles and antenna reflectors) to supply sufficient power and reduce launch costs.

Typically, when constructing a dynamic model of a flexible spacecraft, it is necessary to account for the interaction between the rigid and elastic modes. One important consideration is the prevention of unwanted excitation of the flexible modes while implementing control measures. The performance of attitude control systems (ACSs) can be compromised by various factors, including the unwanted excitation of the flexible modes during the control of the rigid body attitude, together with other external disturbances, measurement and actuator error, and unmodeled dynamics. Thus, the control scheme must provide adequate stiffness and damping to the rigid body modes, as well as actively damp or reject the flexible modes.

Due to their simplicity and reliability, most existing spacecraft attitude control systems rely on proportional-integral-derivative (PID) or PD laws. However, when faced with model uncertainties and variable coupling vibrations or external disturbances, these PID/PD controllers need help to achieve optimal performance for flexible spacecraft.

In this chapter, we will design and evaluate composite attitude controllers for flexible spacecraft, with a focus on a one-axis case study. We will conduct a comparative analysis of three different control schemes: a standalone PD controller, a PD controller integrated with a Disturbance Observer (PD-DOBC) and a PD controller augmented with an Extended State Observer (PD-ESO). The DOBC and ESO schemes are designed to counteract the effects of vibrations from flexible appendages, while the primary role of the PD controller is to maintain and stabilize the spacecraft's attitude. To enhance the accuracy of the proposed methods and optimize the controller and observer gains, a Particle Swarm Optimization (PSO) method has been proposed. This optimization aims to refine the gains, ensuring they are optimal. Simulation results for a flexible spacecraft model will illustrate that the proposed composite control methods, which combine PD control with either DOBC or ESO, significantly enhance the performance of the attitude control system.

4.2. Problem formulation

To simplify the problem, only single-axis rotation is considered. This model can be derived from the nonlinear attitude dynamics of the flexible spacecraft [27, 28]. It is assumed that this model includes one rigid body and one flexible appendage (as shown in Fig 4.1) and the relative elastic spacecraft model is described as:

$$J\ddot{\theta} + F\ddot{\eta} = u + d_1 \tag{4.1}$$

$$\ddot{\eta} + 2\xi\omega_\eta\dot{\eta} + {\omega_\eta}^2\eta + F^T\ddot{\theta} = 0 \tag{4.2}$$

where θ is the attitude angle, J is the moment of inertia of the spacecraft, F is the rigid elastic coupling matrix, u is the control torque, d_1 represents the external disturbance torque, which accounts for the space environmental torques acting on the system, η is the flexible modal coordinate, ξ is the damping ratio, and ω_η is the modal frequency.

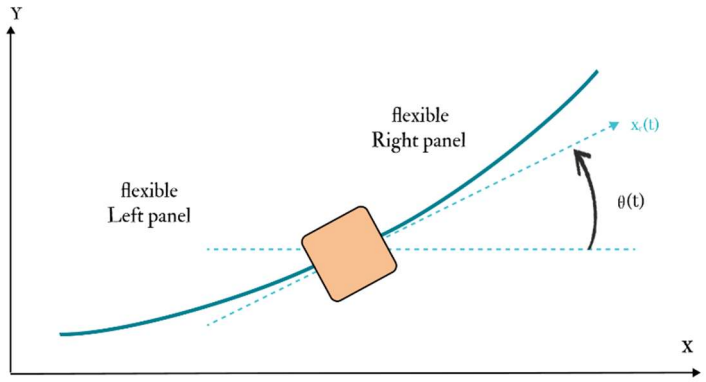

Fig 4.1: Spacecraft with flexible appendages.

Combining Eq (4.1) with Eq (4.2), We can get:

$$(J - FF^T)\ddot{\theta} = F(2\xi\omega_\eta\dot{\eta} + {\omega_\eta}^2\eta) + u + d_1 \qquad (4.3)$$

From Eq (4.3), the item $d_0 = F(2\xi\omega_\eta\dot{\eta} + {\omega_\eta}^2\eta)$ is considered an internal disturbance caused by the elastic vibration of the flexible appendages

Denote $x(t) = [\theta(t), \dot{\theta}(t)]^{\mathrm{T}}$, then Eq (4.3) can be transformed into:

$$\dot{x}(t) = Ax(t) + B_u u(t) + B_f d_0(t) + B_d d_1(t) \qquad (4.4)$$

where, $A = \begin{bmatrix} 0 & 1 \\ 0 & 0 \end{bmatrix}$, $B = B_u = B_d = B_f = \begin{bmatrix} 0 \\ (J - FF^T)^{-1} \end{bmatrix}$

4.3. Flexible Spacecraft Attitude Control System Design

This section analyzes different control strategies for achieving the flexible spacecraft's desired angular attitude and velocity. To accomplish this, a PD controller is employed first. Then, an extended state observer is integrated with the PD controller to enhance the control system's accuracy. Additionally, a disturbance observer is utilized to stabilize the spacecraft's attitude in the presence of internal and external disturbances.

4.3.1. PD Controller

A Proportional-Derived controller is employed to control the spacecraft's attitude. The primary objective of this controller is to achieve and maintain the desired attitude angle and angular velocity while reducing the impact of the unwanted vibrations caused by the spacecraft's flexible appendage. The output signal in the time domain is given by [29]:

$$y(t) = K_p x(t) + K_d \frac{dx(t)}{dt} \tag{4.5}$$

Since PD controllers are widely used in practical systems, especially in attitude control applications, the control is considered as follows:

$$u_c = K_p\,[\theta(t) - \theta ref] + K_d\,\dot{\theta}(t) \tag{4.6}$$

where K_p and K_d are the proportional derivative gains, respectively. Fig 4.2 shows the block diagram of a PD attitude control system applied to a flexible spacecraft.

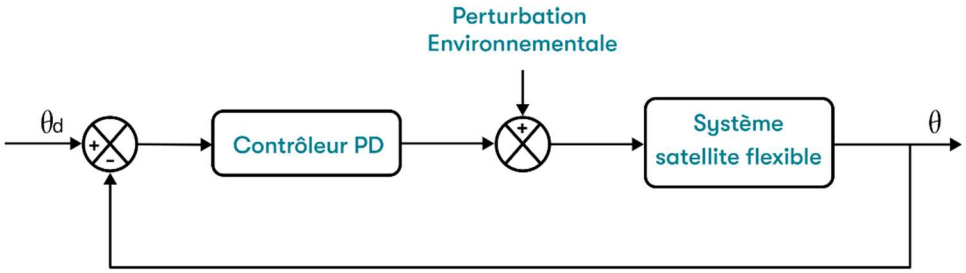

Fig 4.2: Block diagram of PD controller

After introducing the PD controller, we investigate the concept of composite control. This approach combines a controller with an observer to compensate for internal and external disturbances, commonly called lumped disturbances. In this chapter, we give more details of the two observers and how they are utilized within the context of composite control.

4.3.2. Extended State Observer

This observer, known as an extended state observer (ESO), augments the state observer by estimating not only the system states but also lumped disturbances acting on the system, which are treated as an additional "extended state." Estimating these lumped disturbances enables feed-forward compensation in the control design. First, the ESO estimates the disturbances by incorporating them into the observer's state vector. The estimated disturbances can then be compensated for using feed-forward control, attenuating their impact on the system. Subsequently, a PD controller can stabilize the system's attitude, benefiting from the reduced disturbance effects due to the feed-forward compensation. By combining disturbance estimation, feed-forward compensation, and feedback control, the ESO-based control approach enhances disturbance rejection and attitude stabilization capabilities. The scheme of the ESO is represented in the figure below.

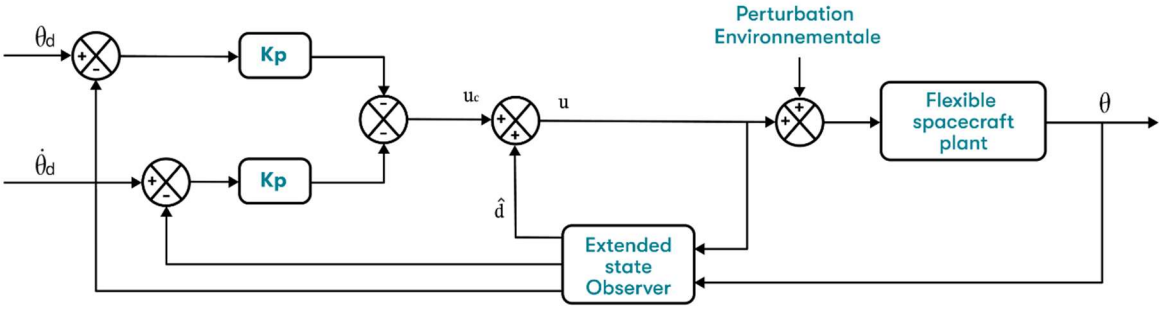

Fig 4.3: Block diagram of composite attitude controller PD-ESO

Let $x_1 = \theta$, $x_2 = \dot{\theta}$, then Eq (4.3) can be transformed into:

$$\begin{cases} \dot{x}_1 = x_2 \\ \dot{x}_2 = B_u u + B_f d \end{cases} \tag{4.7}$$

Define an extended state $x_3 = d$, and system in Eq (4.7) can be augmented as:

$$\begin{cases} \dot{x}_1 = x_2 \\ \dot{x}_2 = B_u u + B_f d \\ \dot{x}_3 = 0 \end{cases} \tag{4.8}$$

In order to estimate the extended states, a linear ESO is generally designed as:

$$\begin{cases} \dot{\hat{x}}_1 = \hat{x}_2 + l_1(x_1 - \hat{x}_1) \\ \dot{\hat{x}}_2 = B_u u + B_f \hat{x}_3 + l_2(x_1 - \hat{x}_1) \\ \dot{\hat{x}}_3 = l_3(x_1 - \hat{x}_1) \end{cases} \tag{4.9}$$

where $\hat{x}_1$, $\hat{x}_2$ and $\hat{x}_3$ are estimates of the state variables x_1, x_2 and x_3 respectively, and $l_1, l_2, l_3 > 0$ are observer gains to be designed. The estimation errors of x_1, x_2 and x_3 are defined as $\tilde{x}_1 = x_1 - \hat{x}_1$, $\tilde{x}_2 = x_2 - \hat{x}_2$ and $\tilde{x}_3 = x_3 - \hat{x}_3$ respectively.

A composite control law is designed as follows:

$$u = u_c - \hat{x}_3 = -K_p \hat{x}_1 - K_d \hat{x}_2 - \hat{x}_3 \tag{4.10}$$

Using the estimation error of x_1, x_2 and x_3 the control law can be reformed as:

$$u = -K_p x_1 - K_d x_2 + K_p \tilde{x}_1 + K_d \tilde{x}_2 - x_3 + \tilde{x}_3 \tag{4.11}$$

Then Eq (4.7) can be transformed as:

$$\begin{cases} \dot{x}_1 = x_2 \\ \dot{x}_2 = -BK_p x_1 - BK_d x_2 + B(K_p \tilde{x}_1 + K_d \tilde{x}_2 + \tilde{x}_3) \end{cases} \tag{4.12}$$

Its state matrix is

$$A_c = \begin{bmatrix} 0 & 1 \\ -BK_p & -BK_d \end{bmatrix} \tag{4.13}$$

The eigenvalues of A_c are calculated as follows:

$$|\lambda I - A_c| = \lambda^2 + B\lambda K_p + BK_d = 0 \tag{4.14}$$

Since $B\lambda K_p$, $BK_d > 0$, we can conclude that all eigenvalues of A_c have negative real part, i.e. the control system is stable asymptotically.

After introducing the Extended State Observer as one of the two methods, we can provide details about the second method, which is the Disturbance Observer-Based Control (DOBC).

4.3.3 Disturbance Observer Based Control

Disturbance Observer-Based Control is a highly effective method in which a disturbance estimator is specifically designed to compensate for disturbances via feedforward control. This approach is exceptionally beneficial for reducing vibrations in systems that are affected by external factors, such as solar panels or fuel sloshing.

For the sake of simplicity, we suppose that the disturbance d_0 in Eq (4.4) is slowly varying and bounded $\lim_{t\to\infty} \dot{d}_0 = 0$

According to system Eq (4.4), we formulate the disturbance observer as

$$\begin{cases} \dot{p}(t) = -LB_d\big(p(t) + Lx(t)\big) - L(Ax(t) + B_u u(t)) \\ \hat{d}_0 = p(t) + Lx(t) \end{cases} \tag{4.15}$$

where p the internal variable vector of the observer, and L the observe gain to be designed.

The error of disturbance observer is defined as $e(t) = d_0(t) - \hat{d}_0(t)$.

According to the practical situation of the flexible spacecraft, we should design an appropriate L to make $e(t) \to 0$.

In the DOBC scheme, the controller can be constructed as $u(t) = u_c(t) - \hat{d}_0(t)$, which is directly described by Fig 4.4 (where $\hat{d}_0(t)$ is the estimation of $d_0(t)$).

As shown in this figure, the composite controller consists of two parts: a feedback control part and a feedforward control part based on a disturbance observer. Feedback control is often used to track and stabilize of the nominal dynamics of the controlled plant. Disturbances and uncertainties on controlled plant are estimated by a disturbance observer and then compensated by a feedforward control.

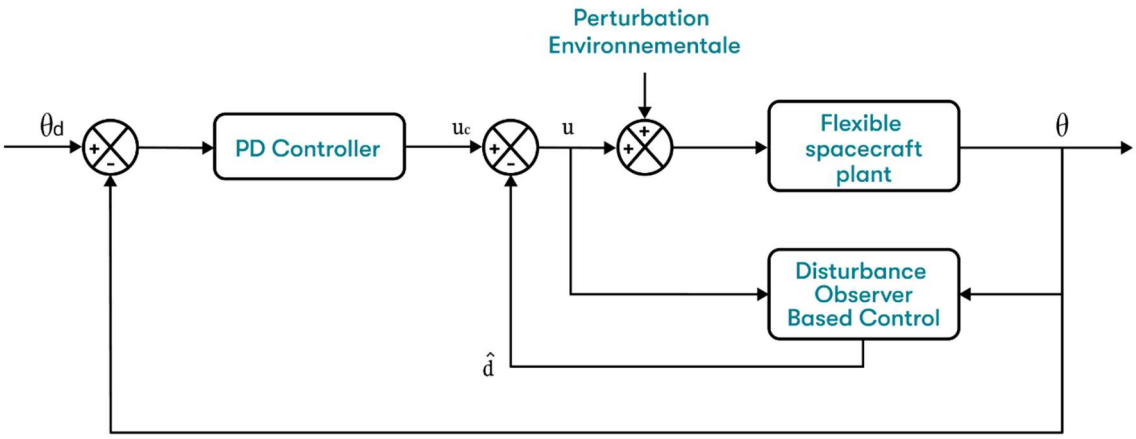

Fig 4.4: Block diagram of composite attitude controller PD-DOBC.

4.4. Stability analysis

To achieve stability of the closed-loop system, some mild assumptions are given as follows.

Assumption 1 Both the lumped disturbance d and its derivative $\dot{d}$ are bounded.

Assumption 2 The lumped disturbances d have constant values in steady-state, i.e. $\lim_{t\to\infty} \dot{d} = 0$ or $\lim_{t\to\infty} d = d_s$ where d_s is a constant vector.

Assumption 3 (A,B_u) is controllable.

The asymptotic stability of DO Eq (4.15) is concluded by the following theorem.

Theorem 1 Suppose that assumption 1 and 3 are satisfied for system Eq (4.4). The disturbance estimates $\hat{d}$ yielded by DO Eq (4.15) can asymptotically track the lumped disturbances d if the observer gain matrix L in Eq (4.15) is chosen such that matrix $-LB_d$ is Hurwitz.

Proof The disturbance estimation error of the DO Eq (4.15) is defined as

$$e_d = \hat{d} - d \tag{4.16}$$

Combining system Eq (4.4), DO Eq (4.15), with estimation error Eq (4.16), gives

$$\dot{e}_d = \dot{\hat{d}} - \dot{d}$$

$$= \dot{p} + L\dot{x} - \dot{d}$$

$$= -LB_d\hat{d} - L(Ax + B_u) + L(Ax + B_u u + B_d d) - \dot{d}$$

$$= -LB_d(\hat{d} - d) - \dot{d}$$

$$= -LB_d e_d - \dot{d} \tag{4.17}$$

It can be verified that the error system Eq (4.17) is asymptotically stable since $-LB_d$ is Hurwitz, is bounded and satisfies $\lim_{t\to\infty} \dot{d} = 0$. This implies that the disturbance estimate of DO can track the disturbances asymptotically.

The bounded-input-bounded-output (BIBO) and asymptotic stabilities of the closed-loop system are shown as follows.

Theorem 2 Suppose that Assumptions 1 and 3 are satisfied for system Eq (4.4). The BIBO stability of system Eq (4.4) under the newly proposed DOBC law is guaranteed if the observer gain L in Eq (4.15) and the feedback control gain K are selected such that both $-LB_d$ and $A + B_u K$ are Hurwitz.

Proof Combining system Eq (4.4), composite control law, with error system Eq (4.17), the closed-loop system is written as

$$\begin{bmatrix} \dot{x} \\ \dot{e}_d \end{bmatrix} = \begin{bmatrix} A - B_u K & -B_u \\ 0 & -LB_d \end{bmatrix} \begin{bmatrix} x \\ e_d \end{bmatrix} + \begin{bmatrix} B_d - B_u & 0 \\ 0 & -1 \end{bmatrix} \begin{bmatrix} d \\ \dot{d} \end{bmatrix} \tag{4.18}$$

Since $-LB_d$ and $A + B_u K$ are Hurwitz, it can be verified that matrix

$$\begin{bmatrix} A - B_u K & -B_u \\ 0 & -LB_d \end{bmatrix}$$

is also Hurwitz. It can be concluded that the closed-loop system is BIBO stable for any bounded d and $\dot{d}$ if K and L are properly selected.

Theorem 3 Suppose that Assumptions 1 and 2 are satisfied for system Eq (4.4). The states of system Eq (4.4) under the composite control law converge to $x_s = -(A - B_u K)^{-1}(-B_u + B_d)\, d_s$ asymptotically if the observer gain L in Eq (4.15) and the feedback control gain K are selected such that both $-LB_d$ and $A + B_u K$ are Hurwitz.

Proof The state error can be constructed as

$$e_x = x - x_s \tag{4.19}$$

Combining system Eq (4.4), composite control law, error system Eq (4.17), with state error Eq (4.18), closed-loop system is given as

$$\begin{bmatrix} \dot{e}_x \\ \dot{e}_d \end{bmatrix} = \begin{bmatrix} A - B_u K & -B_u \\ 0 & -LB_d \end{bmatrix} \begin{bmatrix} e_x \\ e_d \end{bmatrix} + \tag{4.20}$$

$$\begin{bmatrix} B_d - B_u & 0 \\ 0 & -1 \end{bmatrix} \begin{bmatrix} d - d_s \\ \dot{d} \end{bmatrix}$$

Similar with the proof of Theorem 2, it can be verified that

$$\begin{bmatrix} A - B_u K & -B_u \\ 0 & -LB_d \end{bmatrix}$$

is Hurwitz. In addition, it can be obtained from Assumption 2 that $\lim_{t\to\infty}[\, d(t) - d_s] = 0$.

Considering the conditions, it can be shown that the closed-loop system Eq (4.20) is asymptotically stable. This means that with the given conditions the state vector converges to a constant vector x_s asymptotically [30].

4.5. Controller tuning

This section employs pole placement and Particle Swarm Optimization (PSO) tuning strategies to optimize the controller gains. *Pole placement* is a control system design technique used to place the closed-loop poles of a system at desired locations. The PSO algorithm, a bio-inspired metaheuristic optimization technique, tunes the controller gains by iteratively exploring the search space and converging toward the optimal solution that minimizes a predefined cost function.

4.5.1 pole placement

In this section, we introduce a design method often called pole placement or pole-assignment technique. By choosing an appropriate gain matrix for state feedback, it is possible to force the system to have closed-loop poles at the desired locations, provided that the original system is completely state controllable, then poles of the closed-loop system are placed at any desired locations using state feedback and the proper state feedback gain matrix [31].

4.5.2 Particle Swarm Optimization (PSO)

The particle swarm algorithm is based on imitating bird populations, transforming the foraging process into a problem of finding the optimal solution to the problem, and plays an important role in solving multiple system optimization problems. This algorithm is an intelligent parallel group optimization algorithm. Compared with genetic algorithms, it avoids population crossover and mutation operations. The optimization process is simple, the number of parameters is small, and it has the advantages of fast convergence speed and strong global search ability. Therefore, it is often used in complex high-dimensional problems such as function optimization.

First, the operator must specify a specific number of particles and populations, and provide specific velocity and position information for each particle. The fitness function is an important indicator reflecting the motion state of particles. It can be adjusted according to the characteristics of the controller or the response error of the system and serves as the termination condition of the particle optimization process. Changes in the position and velocity of the particle in the motion space are not only related to the inertia weight w, learning factors c_1 and c_2, and random constants r_1 and r_2, but also closely related to the two extreme parameters. One is the individual extreme value P_{best} of the particle, which represents the current best position of the particle, and the other is the global extreme value G_{best} of the group, which represents the current best position in the population. The two extreme parameters indicate the direction for the movement of the particle swarm. The Eq (4.21) and Eq (4.22) are the update formulas for the velocity and position of the particles:

$$v_i(t) = wv_i(t-1) + c_1 r_1 \left(P_{best,i} - x_i(t-1)\right) \quad (4.21)$$

$$+ c_2 r_2 \left(G_{best} - x_i(t-1)\right)$$

$$x_i(t) = x_i(t-1) + v_i(t) \quad (4.22)$$

The select of fitness function is very important for the accuracy of parameter tuning. In order to achieve fast dynamic performance, taking into account the stability and accuracy of the system, a fitness function j composed of ITAE indicators is used. Additionally, the control system's output error is chosen as the integral term.

$$j = \int_0^\infty t|e(t)|dt \quad (4.23)$$

Generally, the smaller the value of the performance index function, the better the parameter optimization effect, in other words, the problem becomes one of determining the function's minimal value.

The optimization process of particles swarm algorithm is shown in Fig 4.5.

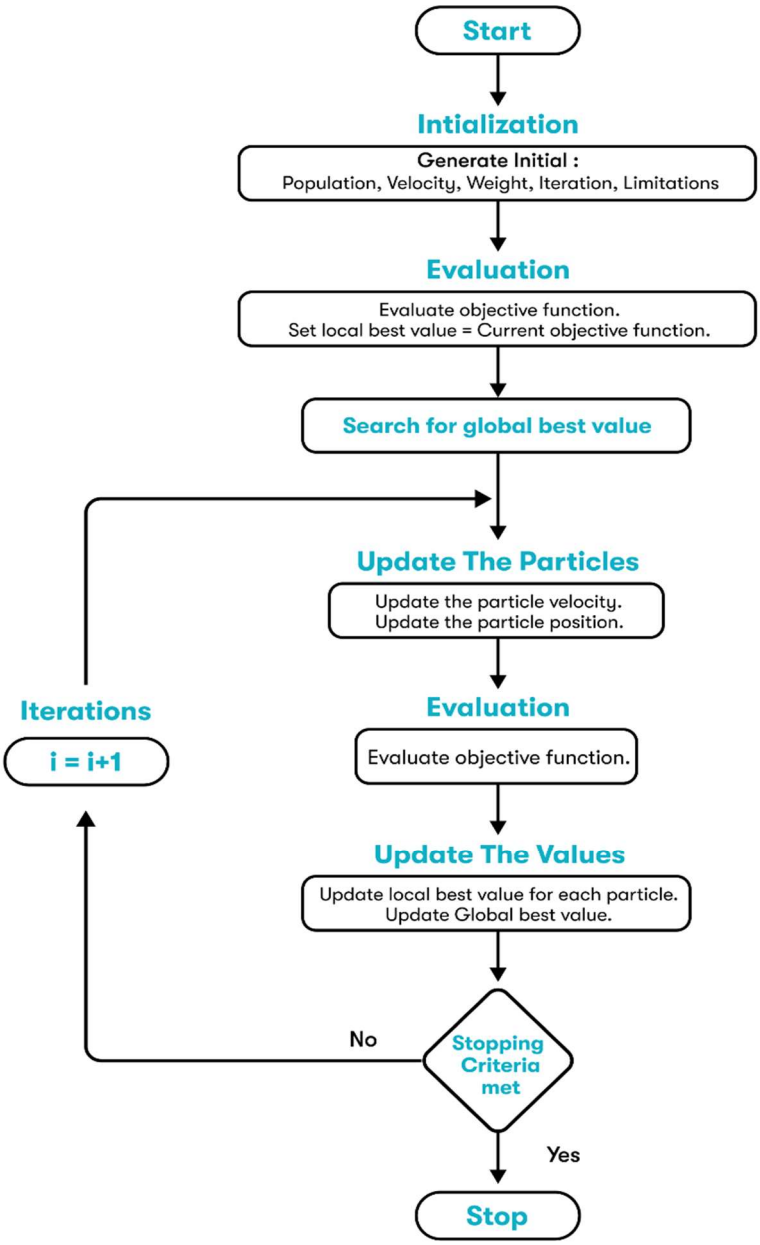

Fig 4.5: Optimization flow chart of PSO.

4.6. Simulation and result analysis

In this section, the effectiveness of the present algorithms is demonstrated by numerical simulations. The effect of the elastic vibration is observed and compensated, and then fine attitude control is obtained. The composite controller has been applied to the attitude control of a spacecraft with flexible appendages.

In the simulation, we only consider the spacecraft attitude stabilization in the roll channel. The moment of inertia of the spacecraft is $J = 440\text{kg.m}^2$, and we suppose that $\omega_1 = \omega_2 = 0.3$ rad/s with damping $\xi_1 = \xi_2 = 0.005$, the coupling coefficients are given as : $F = [1.278 \quad 1.278]$.

The flexible spacecraft is designed to move in the geostationary orbit with the altitude of 36000Km, then the orbit rate $n = 0.0011$ rad/s.

The space environmental disturbance torques acting on the satellite are assumed as

$$\begin{cases} T_{dx} = 4.5 \times 10^{-5}(3\cos nt + 1), \\ T_{dy} = 4.5 \times 10^{-5}(3\cos nt + 1.5\sin nt), \\ T_{dz} = 4.5 \times 10^{-5}(3\cos nt + 1), \end{cases} \text{(Nm)}$$

To guarantee the convergence of the observers, their gain is chosen as:

- For extended state observer $L_e = [240 \quad 8416 \quad 8320]$, so that the corresponding extended state observer poles are $p = [-20 - 4i \quad -20 + 4i \quad -200]$
- For disturbance observer-based control $L = [0 \quad 1481.3]$, so that the corresponding disturbance observer's poles are $p = [38.4876604i \quad -38.4876604i]$

By employing the trial-and-error method, the feedback control gain is designed as $[K_p \quad K_d] = [4.99 \quad 39.91]$. The initial pitch attitude of the space craft is $\theta = 2.8$ deg, $\dot{\theta} = 0.05$ deg/s.

Based on the MATLAB/SIMULINK simulation and in order to improve the speed and the accuracy of tuning parameters, the PSO-PD design method is used to optimize the parameters of the PD controller. In the optimization process, set the number of particle populations to 50, the number of iterations to 200, and the learning factors to be 2. The change curve of the fitness function value is shown in Fig 4.5. From the simulation diagram, it can be seen that when the number of iterations reaches about 103, the control accuracy of the system can be stabilized at about 4.1406.

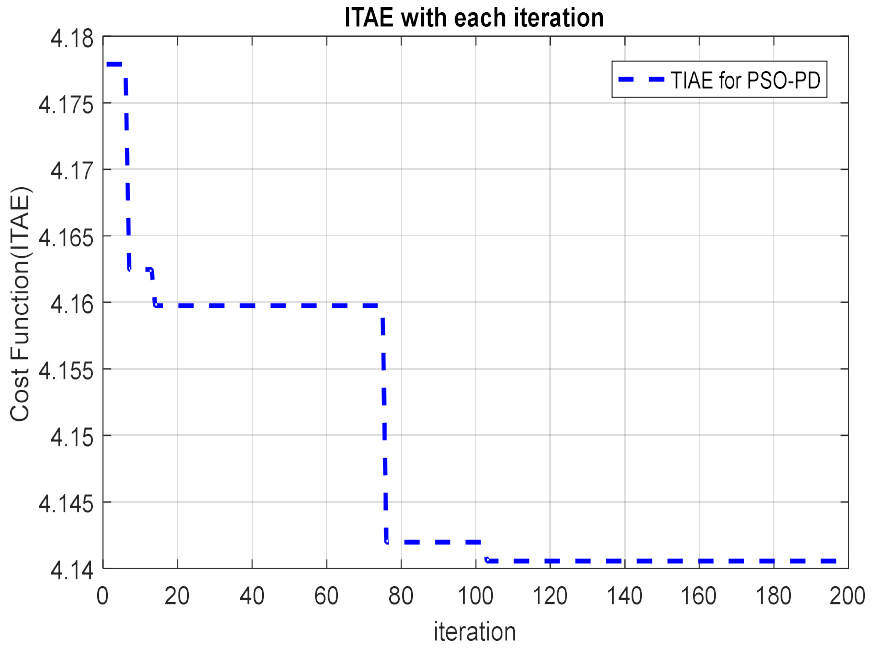

Fig 4.6: Fitness function curve for PD gain

The parameters of the observer are also selected using the PSO. For the ESO set the number of particle populations to 70, the number of iterations to 120, and the learning factors to be 2. The change curve of the fitness function value is shown in Fig 4.6. From the simulation diagram, it can be seen that when the number of iterations reaches about 93, the control accuracy of the system can be stabilized at about 14.83.

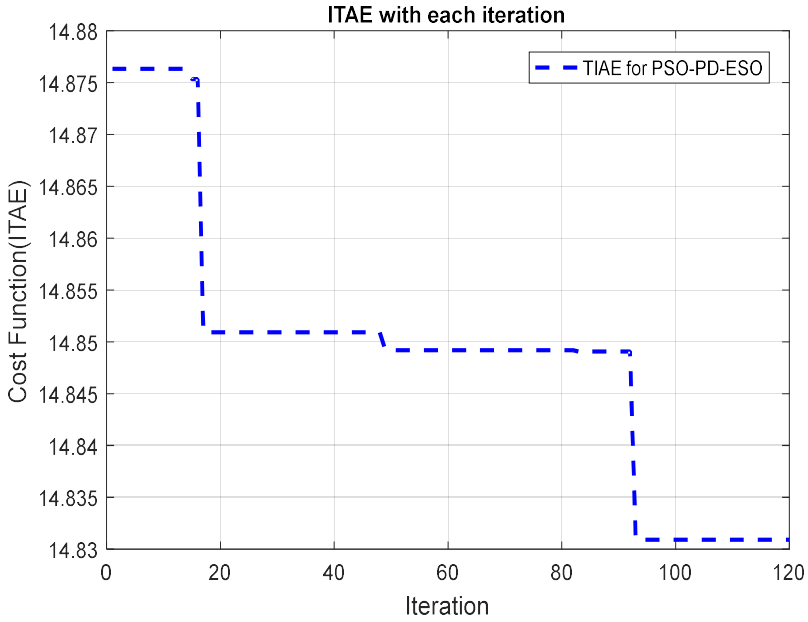

Fig 4.7: Fitness function curve for ESO gain.

Fig 4.7 shows the fitness function curve for the gain of the DOBC. The same parameters are set for the DOBC and the number of particles is set to 90. We can see that when the number of iterations reaches about 111, the system can be stabilized at about 1.353×10^{-12}.

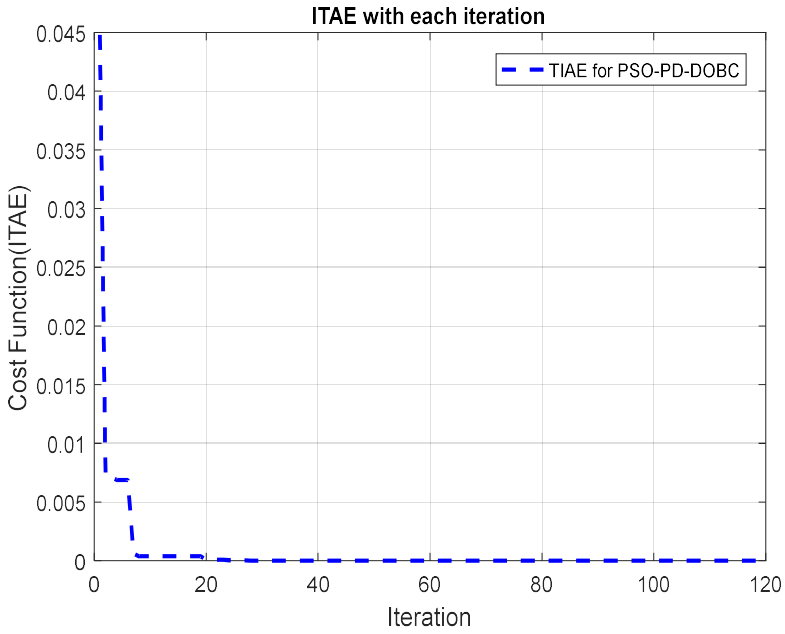

Fig 4.8: Fitness function curve for DOBC gain.

Therefore, the improved parameters of the controllers are shown in the table below:

Table 4.1: Improved parameters of observers and controllers.

Controller part	Control gain	Value
PD	K_p	1000
	K_d	546.1
ESO	l_1	200.5653
	l_2	134 08.81318
	l_3	298815.8488
DOBC	L	[-40 2240.04882]

Table 4.2: RMSE-Controllers

	Symbol	RMSE
PD	Attitude (θ deg)	0.002629
	Velocity ($\dot{\theta}$ deg/s)	3.6721e-05
DOBC	Attitude (θ deg)	0.0002167
	Velocity ($\dot{\theta}$ deg/s)	7.1956e-05
ESO	Attitude (θ deg)	0.0021
	Velocity ($\dot{\theta}$ deg/s)	0.0003352

To analyze the responses and the accuracy of the attitude controller, the most suitable performance metric is the Root Mean Square Error (RMSE).

Table 4.2 shows the RMSE of the attitude angle and its rate of the different controllers using the parameters of the trial-and-error method and pole placement method:

Table 4.3. shows the results of the improved controllers with the PSO method:

Table 4.3: Improved controller results.

	Symbol	**RMS (PSO)**
IPD	Attitude (θ deg)	0.001981
	Velocity (θ̇ deg/s)	1.0067e-04
IDOBC	Attitude (θ deg)	6.944e-5
	Velocity (θ̇ deg/s)	4.0513e-05
ESO	Attitude (θ deg)	0.001783
	Velocity (θ̇ deg/s)	0.0001431

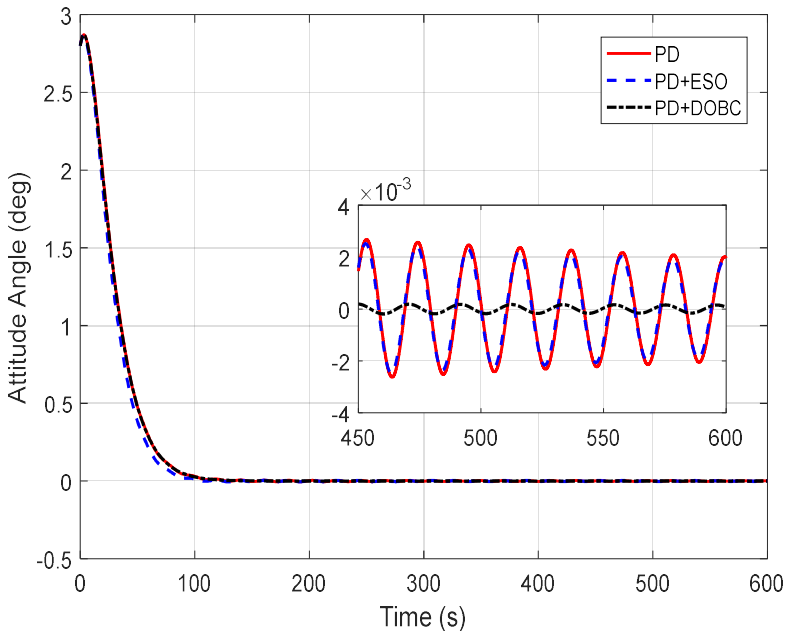

Fig 4.9: Time response of attitude angle.

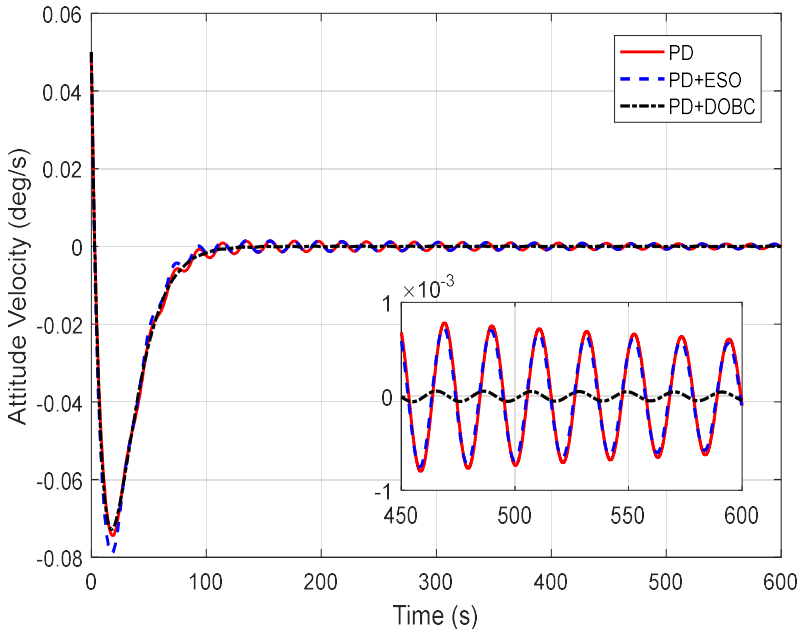

Fig 4.10: Time response of attitude angular velocity.

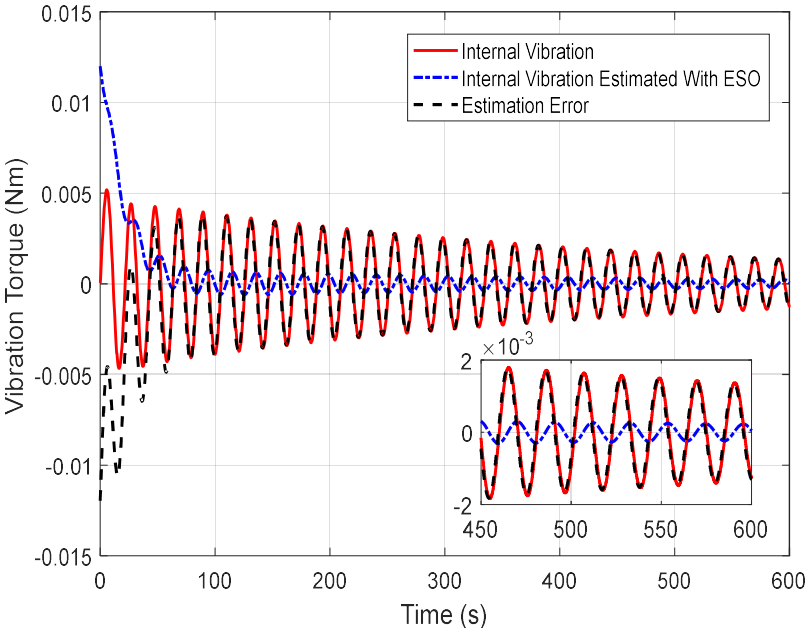

Fig 4.11: Time response of vibration and vibration observed using ESO.

Fig 4.10 illustrates the attitude angle response with the controllers, where we can see that an improved response performance can be guaranteed under the composite controllers. Correspondingly, Fig 4.11 shows the attitude angle velocities converge to the equilibrium point in the presence of flexible vibration.

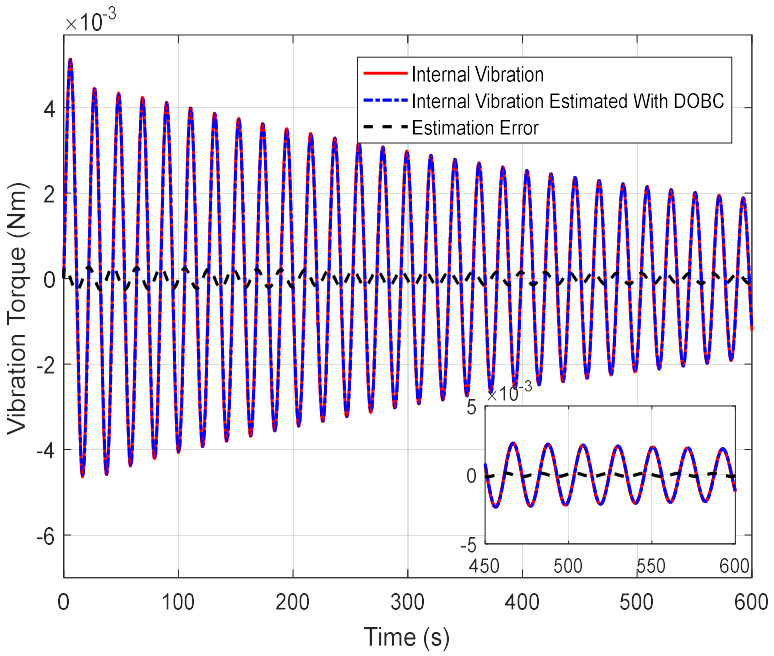

Fig 4.12: Time response of vibration and vibration observed using DOBC.

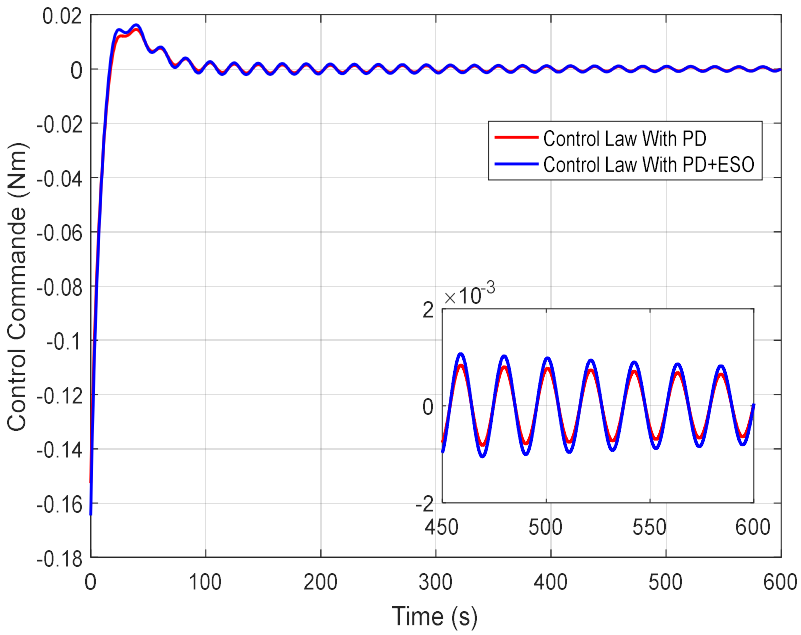

Fig 4.13: Time responses of the control torques with ESO.

Fig 4.12 shows the elastic vibration, its estimation, and the estimation error, respectively, for the two types of composite controllers. One can see that satisfactory tracking performance can be achieved for the vibration from the flexible appendages. With the estimation, the effect of the elastic vibration can be rejected by feed-forward compensation.

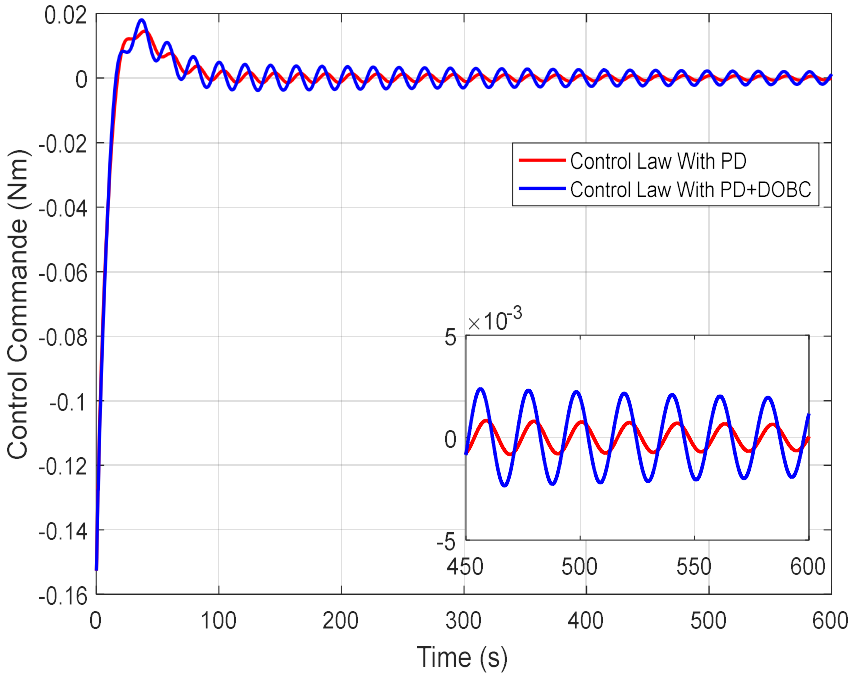

Fig 4.14: Time responses of the control torque with DOBC.

Fig 4.13 and Fig 4.14 illustrate the control torque applied to the flexible spacecraft. It is clear that the composite controllers provide better performance on the system compared to pure PD control. Simulation results demonstrate the effectiveness of the proposed method.

In the last scenario, we present 1000 Monte Carlo simulations by varying the initial conditions randomly from a uniform distribution between ±0.7 degrees for the attitude and ±0.1 degrees/second for the angular rate. The simulation results are presented in Fig 4.15, Fig 4.16 and Fig 4.17, Fig 4.18. From these figures, we can observe that convergence is quickly ensured. Throughout the 1000 Monte Carlo runs, the algorithm did not diverge in any instance.

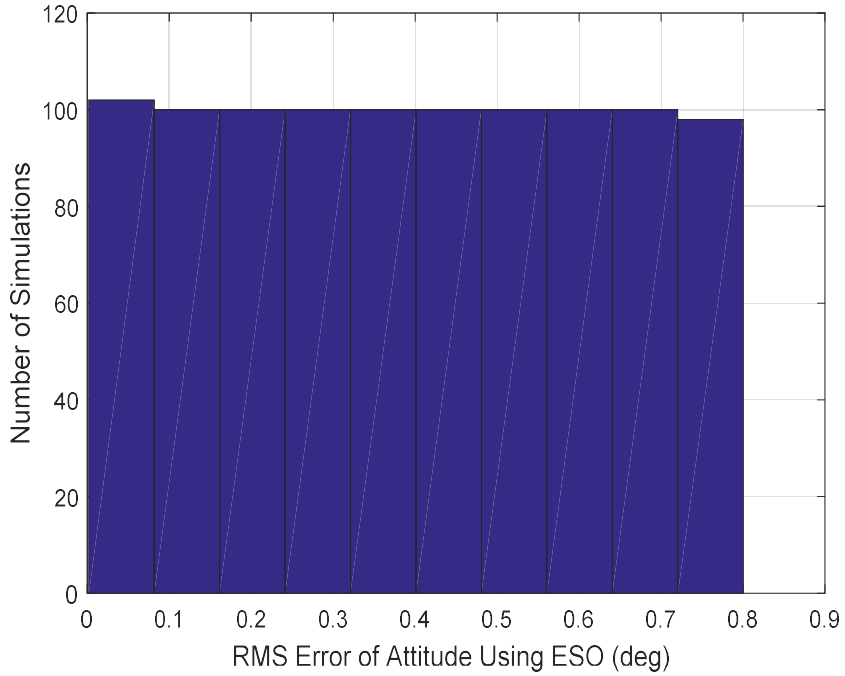

Fig 4.15: Histogram of attitude error standard deviation for 1000 Monte Carlo runs.

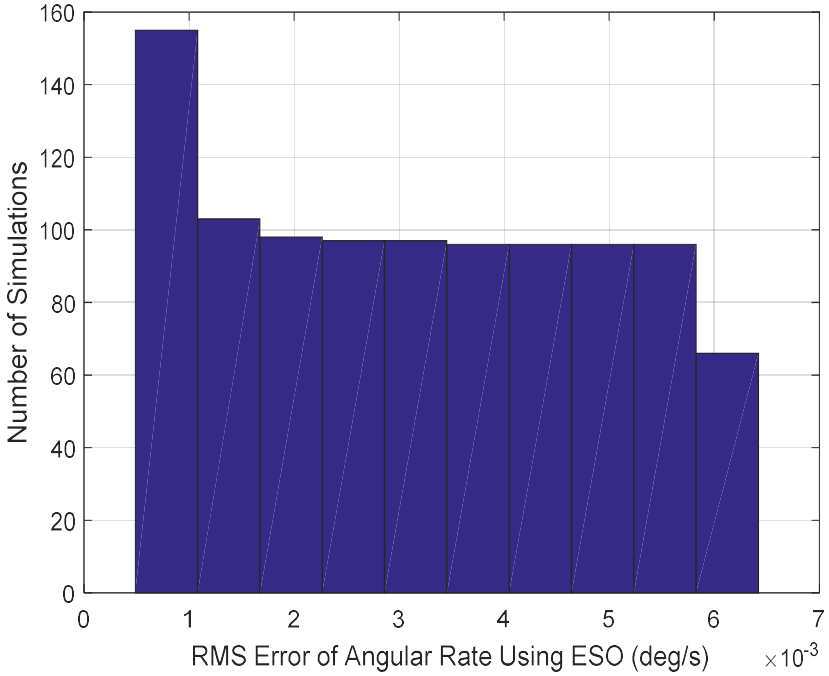

Fig 4.16: Histogram of attitude rate error standard deviation for 1000 Monte Carlo runs.

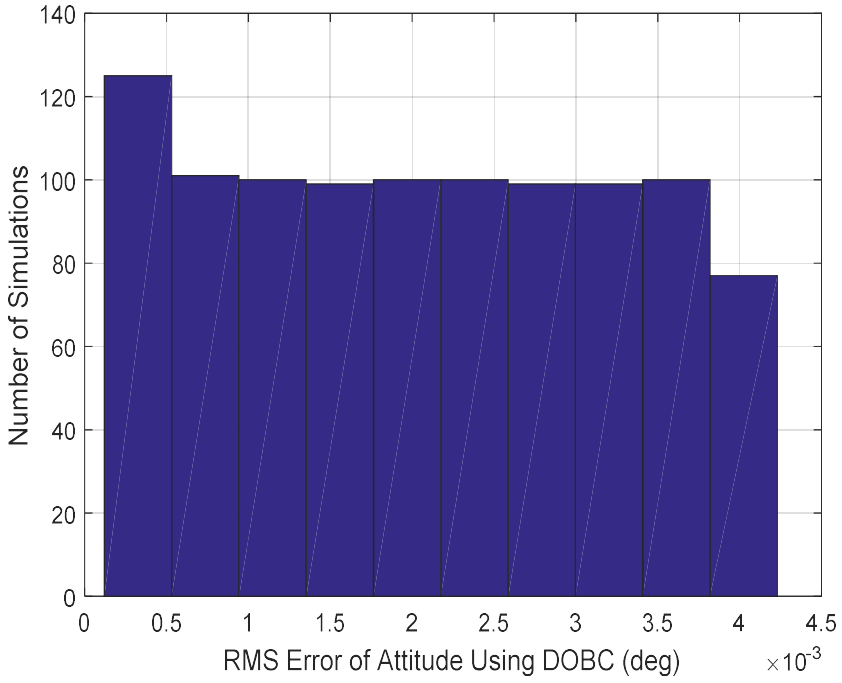

Fig 4.17: Histogram of attitude error standard deviation for 1000 Monte Carlo runs.

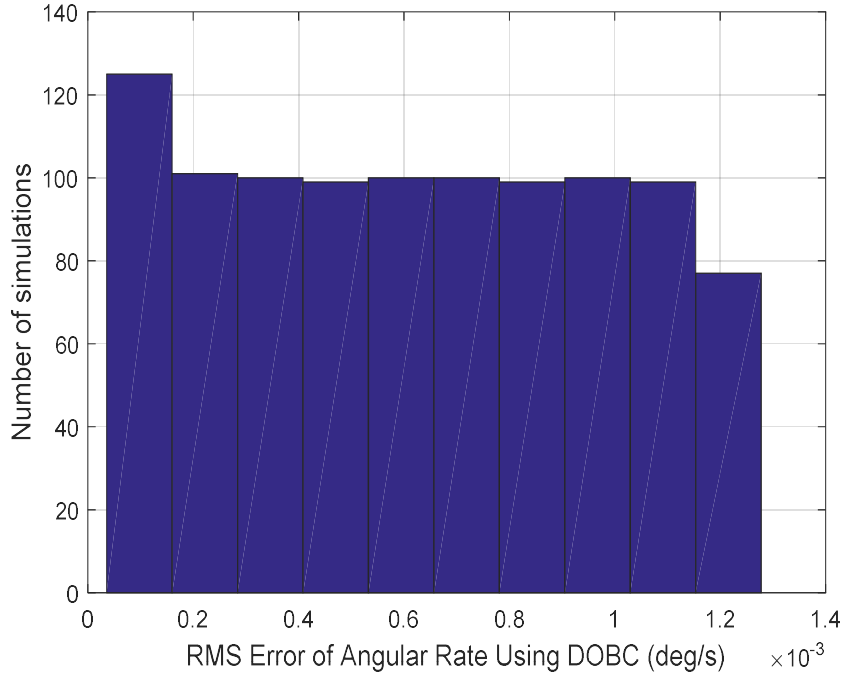

Fig 4.18: Histogram of attitude rate error standard deviation for 1000 Monte Carlo runs.

To conclude, the results of the Monte Carlo simulations demonstrate satisfactory performance, indicating that the adopted controller can effectively counter the undesirable effects produced by uncertainties, leading to high-precision and reliable attitude control.

Based on the simulation results, we can observe the responses and the Root Mean Square Error (RMSE) values for each method. It is evident that the Disturbance Observer-Based Control yields better results than the Extended State Observer. This superiority is reflected in the lower RMSE values for DOBC compared to ESO, suggesting that DOBC is more adept at compensating for internal disturbances in this application. Therefore, DOBC provides more effective compensation for internal disturbances than ESO.

4.7 Conclusion

In conclusion, this chapter explored the application of different control methodologies for single-axis spacecraft attitude control. Specifically, it investigated the performance of Proportional-Derivative (PD) controllers, Extended State Observer (ESO) combined with PD control, and Disturbance Observer-Based Control (DOBC) integrated with PD control.

The results demonstrated that while the PD controller provides a simple and stable approach to attitude control, it struggles to handle disturbances effectively. By integrating ESO or DOBC techniques, the control system gains the ability to estimate and compensate for disturbances, thereby improving performance. It was shown that the DOBC+PD method outperformed the other methods in terms of disturbance rejection and tracking accuracy. Compared to conventional PD control or ESO+PD approaches, the DOBC+PD approach exhibited superior control performance by precisely estimating and compensating for disturbances.

In the next chapter, the study will extend to three-axis attitude control, where the system complexity will be more significant.